

Flash Joule heating to enhance water oxidation of hematite photoanode via mediating with an oxidized carbon overlayer

Guoqing Li^{a,1}, Wei Zhang^{a,1}, Kaiqi Nie^b, Xiaoxin Lv^a, Jiujuun Deng^{a,*}, Hongbing Ji^{c,d,**}

^a Institute for Energy Research, Automotive Engineering Research Institute, Jiangsu University, Zhenjiang, 212013, China

^b Institute of High Energy Physics, Chinese Academy of Sciences, Beijing, 100049, China

^c Research Institute of Sun Yat-sen University in Huizhou, Huizhou, 516081, China

^d Fine Chemical Industry Research Institute, School of Chemistry, Sun Yat-sen University, Guangzhou, 510275, China

ARTICLE INFO

Keywords:

Hematite
Joule heating
Carbon overlayer
Photoelectrochemical
Water oxidation

ABSTRACT

Flash Joule heating technique as an innovative and promising strategy has been extensively utilized to synthesize various functionalized nanomaterials within a very short time. This work describes a facile synthesis of an oxidized carbon overlayer-mediated hematite photoanode through a simple NaH_2PO_2 -immersion followed by a flash Joule heating treatment. It discloses that on account of the high conductivity and abundant oxygen-functionalized carbon groups of carbon overlayer, the surface charge transfer of as-resulted photoanode is greatly facilitated and meanwhile the adsorption strength of water oxidation intermediates on Fe sites is improved. Moreover, the oxidized carbon overlayer could confine sufficient P atoms into the hematite nanostructure to realize P-doping to dramatically promote the bulk charge behaviors. Consequently, benefiting from these multiple effects, an enhanced photocurrent density of 2.07 mA cm^{-2} at 1.23 V vs. RHE is achieved for the as-resulted photoanode. Further, a comparable photocurrent density of 2.37 mA cm^{-2} at 1.23 V vs. RHE is yielded after the loading of FeNiOOH cocatalyst. This study, for the first time, demonstrates the flash Joule heating strategy for the post-treatment of hematite photoanode, which opens up a novel and facile avenue for the development of efficient photoelectrodes.

1. Introduction

Photoelectrochemical (PEC) water splitting has been regarded as one of the most promising routes to convert solar energy into clean hydrogen [1,2]. Among various photoanode candidates, hematite has shown great potential owing to its favorable bandgap ($\sim 2.0 \text{ eV}$) for strong visible light absorption, superior stability in the alkaline electrolyte solution, low cost, and abundance [3–6]. Notably, the theoretical solar-to-hydrogen (STH) conversion efficiency of hematite could reach up to $\sim 16.8\%$, outperforming other commonly-used metal oxide photoanodes [3,5]. However, the STH efficiencies of state-of-art hematite photoanodes are still far below the requirement of large-scale applications ($\text{STH} > 10\%$). Such a discrepancy can be mainly attributed to the intrinsic drawbacks of hematite involving poor electronic conductivity, short charge carriers' diffusion length, very short lifetime of photoexcited holes, and sluggish oxygen evolution reaction (OER) kinetics,

which severely limits the PEC water oxidation performance [3–6].

To solve those issues to boost the conversion efficiency of hematite, considerable efforts have been devoted in past decades and numerous strategies including nanostructuring, element doping, heterojunction building, and surface engineering have been developed [3–10]. Therein, the incorporation of alien atoms (Ti, Sn, Zr, Si, and so on) in hematite nanostructures has turned out to be the most effective one [10–13]. Especially, nonmetallic phosphorus (P) doping has received extensive interest since it can avoid the generation of deep electron trapping sites to render greater promotions on charge mobility [14,15]. Likewise, due to the excellent conductivity and high stability, the decorating of carbon materials (e.g., graphene, carbon quantum dots, organic materials, etc.) onto the surface of hematite photoanode has also been proven viable in greatly boosting photoactivity [16–20]. Recently, surface depositing the element-doped carbon materials with rich active sites towards more efficient hematite photoanodes has acquired significant popularity [21,

* Corresponding author.

** Corresponding author. Research Institute of Sun Yat-sen University in Huizhou, Huizhou, 516081, China.

E-mail addresses: jjDeng@ujs.edu.cn (J. Deng), jihb@mail.sysu.edu.cn (H. Ji).

¹ G. Li and W. Zhang contributed equally to this work.

22]. For instance, Kong et al. reported a nitrogen-doped carbon layer coated hematite photoanode through a hydrothermal procedure followed by a thermal treatment in Argon atmosphere [21]. And owing to the facilitated charge carrier transfer in the bulk and at the electrode/electrolyte interface as well as the accelerated OER kinetics, the as-fabricated photoanode showed an increased photocurrent density of 1.76 mA cm^{-2} at 1.23 V versus reversible hydrogen electrode (vs. RHE) [21]. Also, a cobalt (Co) doped carbon layer on hematite photoanode with a promoted PEC activity has been recently reported, in which the Co-doping carbon overlayer played a triple functional role in improving the surface conductivity, suppressing the surface recombination, and accelerating the OER kinetics [22].

Similar to element-doped carbon materials, surface-oxidized nanocarbon not only preserves the high conductivity but also possesses abundant active sites (oxygen-containing groups) for the strong adsorption of water oxidation intermediates, emerging as a novel and highly active OER electrocatalyst [23–26]. Therefore, it is expected to remarkably enhance the PEC activity of hematite by integrating P-doping and surface treatment of oxidized carbon. However, it's important to note that the construction of such hematite photoanodes in a simple and cost-effective method is still a challenge. In this respect, flash Joule heating provides a feasible route since its rapid heating and cooling rates could render the synthesis process more facile and more efficient [27]. Practically, flash Joule heating as an innovative and promising technique has been extensively applied to fabricate various functionalized nanocarbon materials (e.g., graphene) within a very short time [28,29].

Inspired by these ideas, herein, an oxidized carbon overlayer confined P-doping hematite (defined as P-Fe₂O₃-Joule) photoanode is fabricated through a simple NaH₂PO₂-immersion followed by a high-temperature-shock treatment using the flash Joule heating technique. It demonstrates that during the high-temperature-shock processes, the carbon atoms could be detached from the graphite paper substrate to form a thin carbon layer on the surface of NaH₂PO₂-soaked hematite nanostructure. Further characterizations find that the carbon overlayer contains abundant oxygen-functionalized carbon groups (carbonyl, hydroxyl, and carboxylic groups), which not only enables a better electrolyte affinity for improving the surface charge transfer but also enhances the adsorption strength of *O, *OH, and *OOH intermediates on Fe sites for promoting the OER kinetics. Moreover, it has been disclosed that the high temperature of Joule-heating treatment could stimulate the decomposition of NaH₂PO₂ precursor and then dope P atoms into the hematite lattice due to the confinement of outer carbon layer. As a result, compared to the P-doping photoanode prepared by conventional muffle-sintering (defined as P-Fe₂O₃-Muffle), the P-Fe₂O₃-Joule photoanode exhibits a drastically increased carrier density, resulting in a promoted bulk charge behavior. Eventually, owing to these multiple effects, the P-Fe₂O₃-Joule photoanode yields an increased photocurrent density of 2.07 mA cm^{-2} at 1.23 V vs. RHE, which is about 2.4 and 1.7 times higher than those of pristine Fe₂O₃ and P-Fe₂O₃-Muffle films, respectively. Furthermore, after the loading of FeNiOOH cocatalyst, a comparable photocurrent density of 2.37 mA cm^{-2} at 1.23 V vs. RHE is achieved. This study first demonstrates a novel post-treatment strategy for hematite photoanode through the flash Joule heating technique, which opens a facile and effective avenue toward the development of efficient photoelectrodes.

2. Experimental section

2.1. Synthesis of hematite photoanodes

The pristine Fe₂O₃ photoanode was synthesized through a modified hydrothermal method [9,30]. First, an aqueous solution for the growth of FeOOH film was prepared by dissolving 75 mM iron chloride hexahydrate (FeCl₃·6H₂O, Sinopharm Chemical ReagentCo., Ltd) and 50 mM glucose (C₆H₁₂O₆, Sinopharm Chemical ReagentCo., Ltd) in 80 mL

deionized water. Subsequently, the mixed solution was transferred in a 100 mL Teflon-lined stainless-steel autoclave, and then a piece of cleaned fluorine-doped tin oxide glass (FTO, 50 mm × 30 mm × 1.6 mm, < 15-Ω sq⁻¹, Solar Energy Technology Co., Ltd, Wuhan Jingde, China) was placed in the autoclave. After that, the hydrothermal reaction was performed at 100 °C for 4 h in an oven. After cooling down to room temperature, the FeOOH film grew on the FTO substrate was taken out and rinsed with deionized water, and then sintered at 550 °C for 2 h and 750 °C for additional 15 min to obtain the pristine Fe₂O₃ photoanode.

For the fabrication of P-Fe₂O₃-Joule photoanode, the as-obtained pristine Fe₂O₃ was first soaked in a 50 mL NaH₂PO₂ aqueous solution (concentration from 0.4 to 6 mg/mL) and sonicated for 5 min. Then, after drying at room temperature (~30 min), the NaH₂PO₂-treated Fe₂O₃ photoanode was placed face down into two layers of graphite papers (100 mm in length, 25 mm in width, and 0.2 mm in thickness). Afterward, these graphite papers were connected to the electrical contacts of Joule heating equipment (Hefei in-situ technology Co., Ltd., China) and then sintered under continuous vacuum pumping. During this procedure, the set temperature of Joule heating was achieved by adjusting the output electric current from 60 to 80 A, while the sintering time was realized by regulating the cycles of high-temperature-shock treatment. After the sintering, the photoanode was thoroughly rinsed with deionized water. For the comparison, the P-Fe₂O₃-Muffle photoanode was synthesized by sintering the NaH₂PO₂ solution-soaked Fe₂O₃ photoanode in a muffle at 750 °C for 15 min (ramp rate: 10 °C min⁻¹), the solution concentration and treatment-time for the NaH₂PO₂ soaking are the same as those of P-Fe₂O₃-Joule photoanode. Also, the Fe₂O₃-Joule photoanode has been prepared through the same procedures as those of the P-Fe₂O₃-Joule photoanode except that without the pre-soaking of NaH₂PO₂ solution.

For the deposition of FeNiOOH cocatalyst, a facile electrodeposition method reported in our previous work was adopted [31].

2.2. Structural characterizations

Scanning Electron Microscope (SEM, FEI Quanta FEG 250) and high-resolution Transmission Electron Microscopy (HRTEM, JEOL 2100F) were employed to acquire the morphologies of as-fabricated photoanodes. The HRTEM samples were prepared by mechanically scraping from the surface of as-fabricated photoanodes with a blade, and then transferring directly onto a carbon-film-supported copper grid. The phase structure and crystallinity of as-fabricated photoanodes were examined by X-ray Diffraction (XRD, Shimadzu XRD-6000). FTIR measurements were performed on Thermo Scientific Nicolet iS20. The electronic structures and components of all photoanodes were characterized by X-ray Photoelectron Spectrometer (XPS, SHIMADZU AXIS-Ultra DLD) and X-ray absorption spectroscopy (XAS, Beijing Synchrotron Radiation Facility (Beamline 4B9B)) measurements.

2.3. PEC measurements

The PEC performance of as-fabricated hematite photoanodes was evaluated in a three-electrode cell with a linear sweep voltammetry (LSV) method at the scan rate of 50 mV s⁻¹. The photoanode covered by non-conductive hycol epoxy was used as the working electrode, Pt wire as the counter electrode, and Ag/AgCl electrode as the reference electrode. The NaOH aqueous solution (1 M, pH ≈ 13.6) was used as the electrolyte. The LSV curves were recorded by CHI 660E electrochemical workstation under 100 mW cm⁻² light irradiation (fixed by Thorlabs PM100D power meter) provided by a 300 W Xenon lamp (PLS-FX300HU, Beijing Perfectlight Technology Co., Ltd.) equipped with AM 1.5G filter. Mott-Schottky (M – S) plots were collected with a voltage of 5 mV at a frequency of 1 kHz under dark conditions. Intensity modulated photocurrent spectroscopy (IMPS) measurements were performed using Zahner PP 211 CIMPS (Zahner-Elektrik) GmbH & Co.KG, Kronach, Germany) at different potentials from 0.9 V to 1.6 V vs. RHE. The spectra

were recorded under irradiation with monochromatic light with a wavelength of 561 nm and a fixed intensity of 100 mW cm^{-2} . A modulation of 10% in light intensity was applied, over a frequency range from 100 kHz to 0.1 Hz. Electrochemical Impedance Spectra (EIS) experiments were conducted using CHI 660E electrochemical workstation at 1.23 V vs. RHE under illumination with an AC amplitude of 50 mV and a frequency that ranged from 100 kHz to 0.1 Hz. Tafel plots were obtained from polarization LSV data measured at a scan rate of 1 mV s^{-1} and the potential was iR compensated (the solution resistance was determined from electrochemical impedance data).

3. Results and discussion

Fig. 1 illustrates the preparation of P-Fe₂O₃-Joule photoanode through the flash Joule-heating technique. It is clear that upon applying a current to the graphite paper substrate, temperatures as high as 800 °C could be reached in a very short time (~2 s). Under this circumstance, the carbon atoms could be etched and detached from the graphite paper substrate and then deposited to the surface of NaH₂PO₂-soaked hematite photoanode to form an oxidized carbon overlayer. Meanwhile, the high temperature acquired also offers sufficient energy to decompose the NaH₂PO₂ precursor to generate phosphine (PH₃) gas around the hematite film (Fig. 1c). During this procedure, the confinement of outer

carbon layer incorporates sufficient P atoms in the hematite nanostructure to realize P-doping. By contrast, for the P-Fe₂O₃-Muffle photoanode, the NaH₂PO₂ precursor will be directly oxidized to form phosphate groups on the surface due to the lack of confinement and protection in the conventional Muffle synthesis, as displayed in Fig. 1c.

Fig. S1 displays the X-ray diffraction (XRD) patterns of as-prepared photoanodes, wherein all photoanodes exhibit typical crystalline structures of $\alpha\text{-Fe}_2\text{O}_3$ (JCPDS No. 33-0664), confirming the successful formation of hematite phase. Additionally, after subtracting the XRD peaks derived from the FTO substrate, no diffraction peaks belonging to carbon phases are observed for the P-Fe₂O₃-Joule photoanode, which might associate with the ultrathin and amorphous features of oxidized carbon overlayer. Fig. 2a, b, and c present the scanning electron microscopy (SEM) images of pristine Fe₂O₃, P-Fe₂O₃-Muffle, and P-Fe₂O₃-Joule photoanodes, respectively. All the photoanodes exhibit the resembling worm-like nanostructures, manifesting that the post-annealing treatments via flash Joule-heating and conventional muffle-sintering don't alter the morphologies and gran sizes of hematite nanostructures. High-resolution transmission electron microscopy (HRTEM) characterizations have also been conducted to investigate the subtle structure of the P-Fe₂O₃-Joule photoanode. As demonstrated in Fig. 2d and e, an apparent carbon layer compactly coated on the surface of hematite nanoparticle is found, and the clear lattice spacings of 0.25

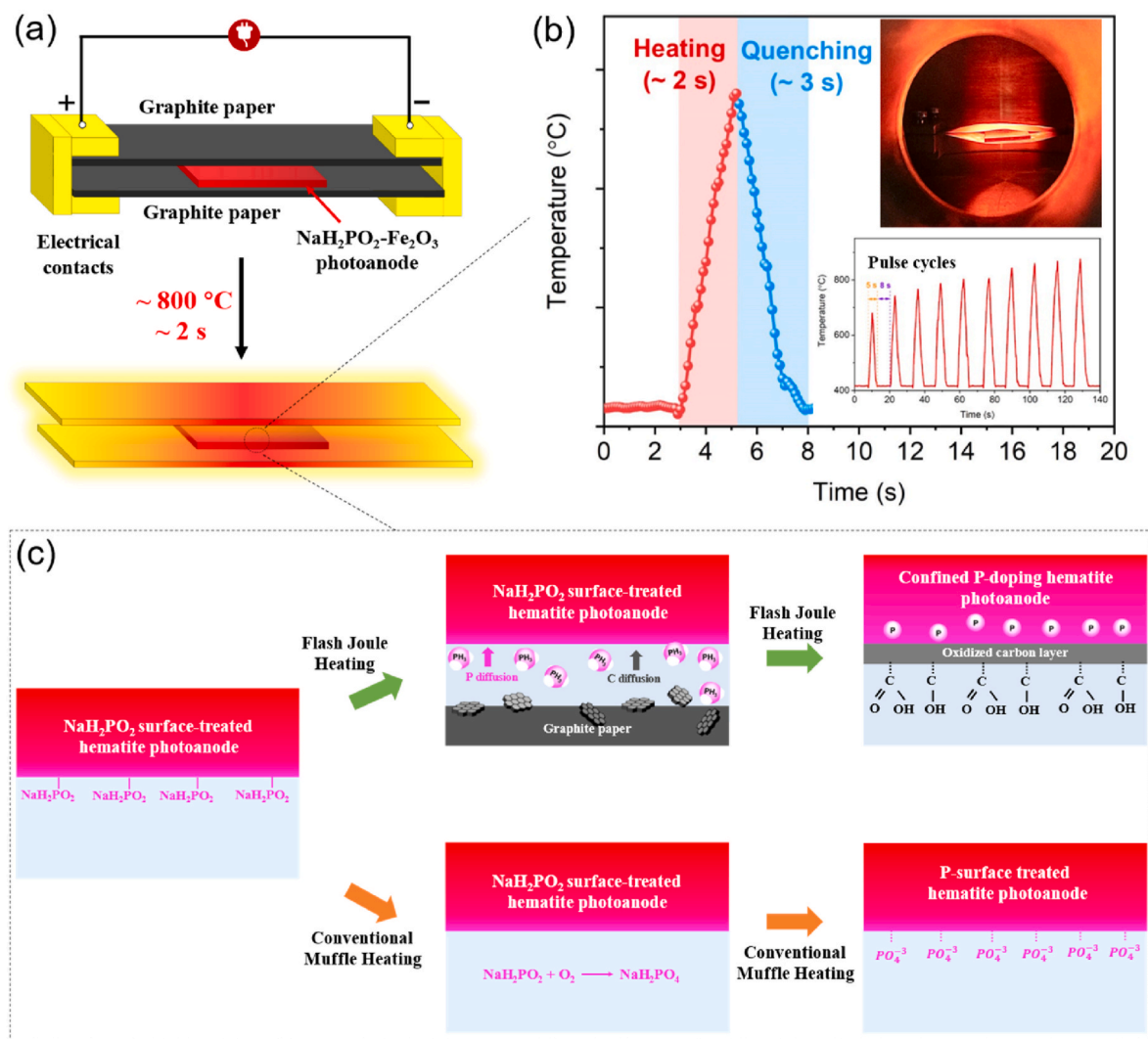


Fig. 1. (a) Schematic illustration for the fabrication of P-Fe₂O₃-Joule photoanode, (b) temperature-time curves of high-temperature-shock treatments, (c) reaction procedure comparison between flash Joule heating technique (P-Fe₂O₃-Joule) and conventional muffle syntheses (P-Fe₂O₃-Muffle). (A colour version of this figure can be viewed online.)

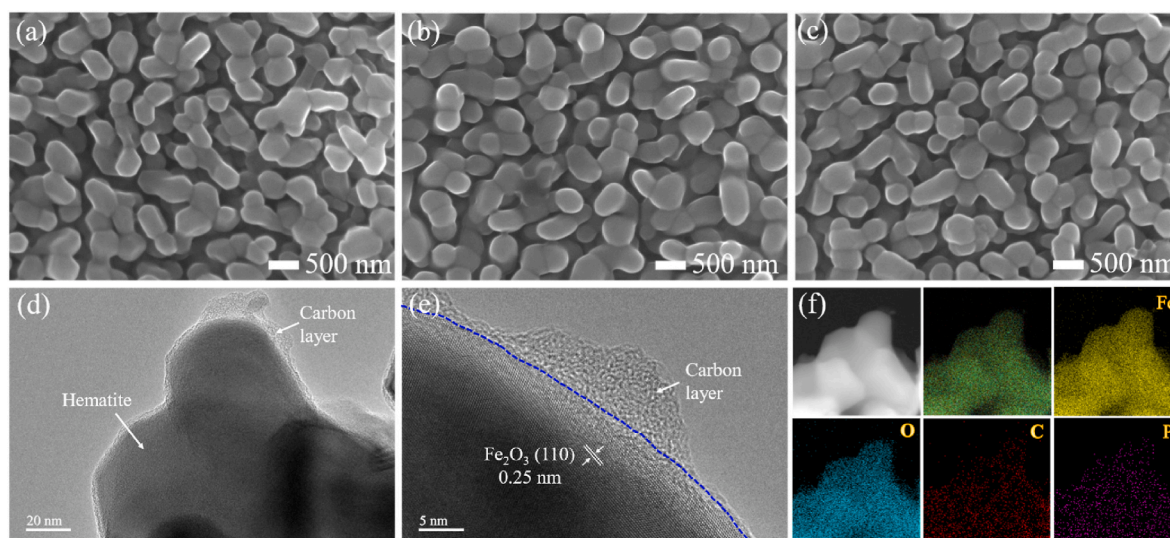


Fig. 2. SEM images of (a) pristine Fe_2O_3 , (b) $\text{P-Fe}_2\text{O}_3$ -Muffle, and (c) $\text{P-Fe}_2\text{O}_3$ -Joule photoanodes, and (d, e) HRTEM images and (f) element mappings of $\text{P-Fe}_2\text{O}_3$ -Joule photoanode. (A colour version of this figure can be viewed online.)

nm also match well with the (110) plane of hematite. Fig. 2f displays the HRTEM element mappings of the $\text{P-Fe}_2\text{O}_3$ -Joule photoanode, in which the homogeneous distributions of C, O, Fe, and P elements further confirm the coating of carbon overlayer and the incorporation of P atoms. Overall, above analyses demonstrate that through the high-

temperature-shock treatment based on the flash Joule heating technique, a carbon overlayer-coated and P-doped hematite photoanode was successfully synthesized. More notable, considering the high conductivity of carbon overlayer and the improved charge mobility originating from P-doping, the charge transfer in the bulk and surface of the

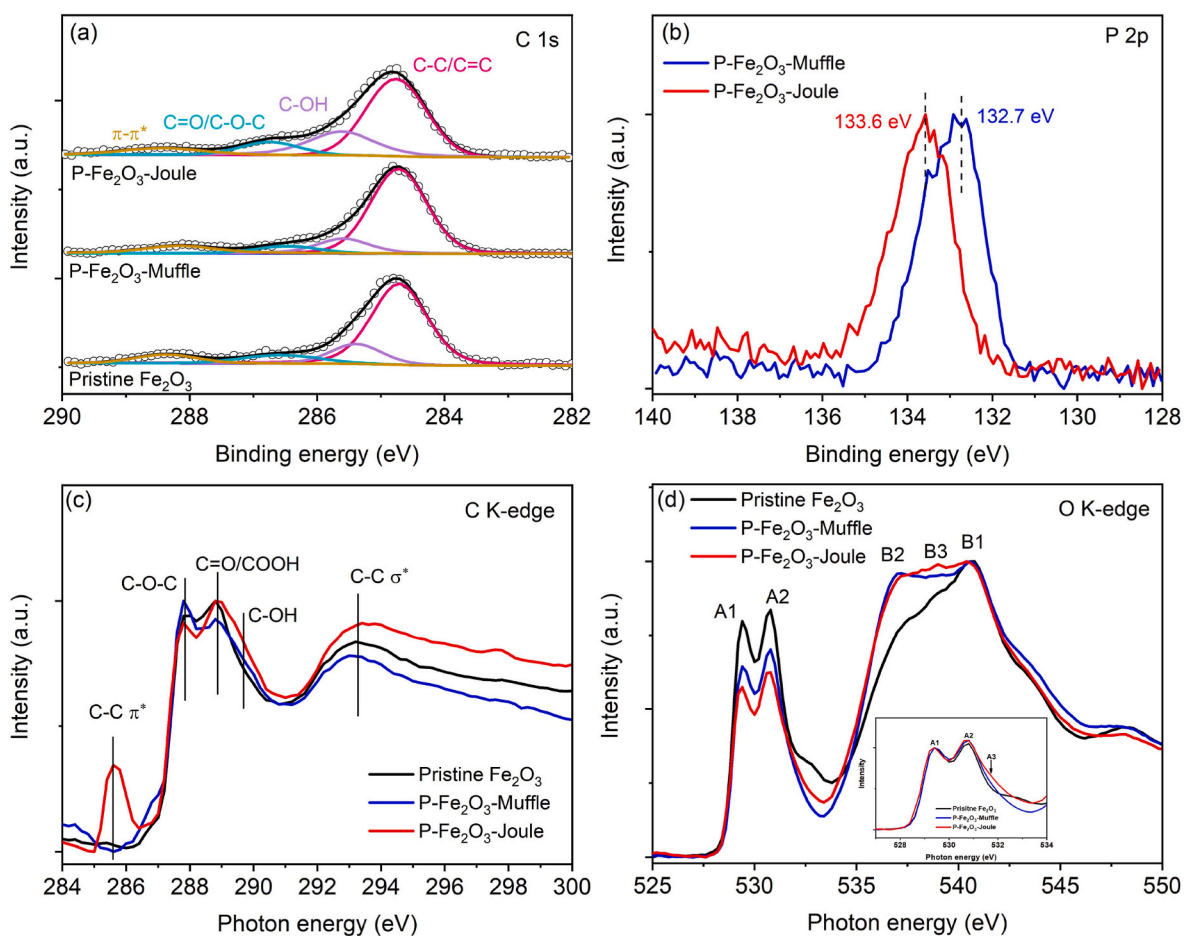


Fig. 3. High-resolution C 1s XPS (a) and P 2p XPS spectra (b), and XAS spectra at C K-edge (c) and O K-edge (d) of pristine Fe_2O_3 , $\text{P-Fe}_2\text{O}_3$ -Muffle, and $\text{P-Fe}_2\text{O}_3$ -Joule photoanodes. (A colour version of this figure can be viewed online.)

P-Fe₂O₃-Joule photoanode will be significantly facilitated, contributing to an enhanced PEC water oxidation performance.

To provide more compelling evidence on the deposition of oxidized carbon overlayer and the incorporation of P atoms, X-ray photoelectron spectroscopy (XPS) and X-ray absorption spectroscopy (XAS) characterizations of as-fabricated photoanodes were carried out. As shown in the survey XPS spectra in Fig. S2a, obvious C, O, Fe, and Sn signals are observed in the pristine Fe₂O₃, P-Fe₂O₃-Muffle, and P-Fe₂O₃-Joule photoanodes, suggesting the successful formation of hematite phase in all photoanodes. In addition, two strong P 2p and P 2s peaks are detected in P-Fe₂O₃-Muffle and P-Fe₂O₃-Joule photoanodes while they are not found in the pristine Fe₂O₃ film, indicating the introduction of P species in both samples. Fig. 3a shows the high-resolution C 1s XPS spectra of as-fabricated hematite photoanodes, in which four deconvoluted peaks corresponding to C-C/C=C groups, C-OH groups, C=O/C-O-C groups, and π - π^* shake-up satellites are observed [32,33]. Relative to pristine Fe₂O₃ and P-Fe₂O₃-Joule photoanodes, P-Fe₂O₃-Joule photoanode exhibits higher contents of C-OH and C=O/C-O-C species, implying that there are more oxygen-functionalized carbon groups in the P-Fe₂O₃-Joule photoanode. Fig. 3b displays the high-resolution P 2p XPS spectra of P-Fe₂O₃-Joule and P-Fe₂O₃-Muffle photoanodes, in which the P-Fe₂O₃-Joule photoanode exhibits a single P 2p peak centered at ~133.6 eV, matching well with those of FePO₄ in literature [34,35]. But for the P-Fe₂O₃-Muffle photoanode, a lower P 2p binding energy of ~132.7 eV is found and which is consistent with the values for phosphates (132.1–132.9 eV, such as NaH₂PO₄) [34]. This difference suggests that on account of the confinement of carbon overlayer, sufficient P atoms were incorporated in hematite nanostructures to generate the Fe-O-P like components in P-Fe₂O₃-Joule photoanode, whereas most of the NaH₂PO₂ precursor would be directly oxidized to form the phosphate species on the surface of P-Fe₂O₃-Muffle photoanode due to the lack of protection in the sintering process [36]. This finding is further evidenced by high-resolution O 1s and Fe 2p XPS spectra. As shown in Fig. S2b, the O 1s XPS spectra demonstrate that relative to pristine Fe₂O₃ film, there is an obvious shift in the binding energy of lattice O²⁻ peak (corresponding to Fe-O bond) of P-Fe₂O₃-Joule photoanode and which can be ascribed to the higher electronegativity of P atoms in P-O bonds than that of Fe atoms in Fe-O bonds [35]. In comparison, an O²⁻ peak located at the same binding energy as that of pristine Fe₂O₃ film is observed in the spectrum of P-Fe₂O₃-Muffle photoanode. Additionally, a strong peak centered at 531.4 eV corresponding to PO₄³⁻ group also appears in the P-Fe₂O₃-Muffle photoanode [37,38]. These observations further indicate that P atoms mostly exist as surface phosphate species for P-Fe₂O₃-Muffle photoanode but P-doping for P-Fe₂O₃-Joule film. Fig. S2c shows the high-resolution Fe 2p XPS spectra of as-fabricated hematite photoanodes. Since P-incorporation could induce larger charge accumulation on P than on Fe due to the higher electronegativity of P atom (2.19) than Fe atom (1.83), the P-Fe₂O₃-Joule photoanode exhibits higher binding energies of Fe 2p_{3/2} and Fe 2p_{1/2} peaks than those of the pristine Fe₂O₃ film [39,40]. On the contrary, no obvious changes in the binding energies of Fe 2p peaks of P-Fe₂O₃-Muffle photoanode are observed because P atoms mainly exist as surface phosphates groups.

XAS characterizations have also been carried out to further probe the electronic structures of as-fabricated photoanodes. As displayed in C K-edge XAS spectra in Fig. 3c, two pronounced features are corresponding to C-C π^* (285.6 eV) and C-C σ^* (293.3 eV) bonds from the carbon ring structure in P-Fe₂O₃-Joule photoanode, implying the presence of sp² carbon structure [22,41]. In contrast, for pristine Fe₂O₃ and P-Fe₂O₃-Muffle photoanodes, the disappearance of typical C-C π^* peak is indicative of amorphous structure and those less-originated carbon species due to the surface adsorption from the atmosphere. Also, it can be seen that there are additional features located between 287 eV and 290 eV in the C K-edge XAS of P-Fe₂O₃-Joule photoanode, which generally originate from different oxygen functionalized carbon groups: C-O-C at 287.8 eV, carboxyl carbon (C=O/COOH) at 288.8 eV, and

C-OH at 289.7 eV [41,42]. These features are indicative of the successful formation of an oxidized carbon overlayer in the P-Fe₂O₃-Joule photoanode. Fig. 3d shows the O K-edge XAS spectra of the pristine Fe₂O₃, P-Fe₂O₃-Joule, and P-Fe₂O₃-Muffle photoanodes, wherein the pre-peaks located at ~530 eV (labeled as A1 and A2) could be ascribed to the transitions from O 1s state to the hybridized O 2p-Fe 3d state while the main feature B1 at ~540 eV is originated from the hybridization of O 2p and Fe 4sp states [5,43]. In addition, there is a broad peak B2 (~537 eV) in the spectra of P-Fe₂O₃-Muffle and P-Fe₂O₃-Joule photoanodes, and which could be assigned to the P-O bands from the surface phosphate groups and P-doping (Fe-O-P), respectively [44]. Moreover, for the P-Fe₂O₃-Joule photoanode, there is an increased shoulder A3 at ~531.7 eV (insert in Fig. 3d) and a new peak B3 at ~539 eV in the O K-edge XAS spectrum, which can be ascribed to COOH (or C=O π^*) and C-O groups, respectively [41]. In addition, the O K-edge XAS spectra also show that the P-Fe₂O₃-Muffle photoanode exhibits reduced pre-peaks (A1 and A2) compared with pristine Fe₂O₃ film, which can be assigned to the formation of surface phosphates groups to donate electrons to the O 2p orbital [45,46]. More notable, since there are sufficient P atoms in the hematite lattice, the O 2p-Fe 3d hybridized orbitals of P-Fe₂O₃-Joule photoanode are more strongly modulated, resulting in the lowest intensities of pre-peaks [45,46]. Fig. S3 shows the P L-edge XAS spectra of as-obtained photoanodes, where several distinct peaks are observed. Peak A at the low energy side corresponds to the transitions from spin-orbit split P 2p electrons into the first unoccupied 3 s-like antibonding state. Broad peak B at higher energy could be ascribed to 2p to 3d transitions in elemental P, and it is known as a shape resonance peak [47,48]. Peaks C and D develop from a second-order C K-edge radiation, probably originating from beamline and sample contamination [49,50]. It is clear that there are no P-C bonds in the P L-edge XAS of the P-Fe₂O₃-Joule photoanode, eliminating the possibility of P doping in the carbon overlayer. Moreover, it has been found that peak B appears at ~146.8 eV for P-Fe₂O₃-Muffle while it locates at ~147.4 eV for P-Fe₂O₃-Joule, which is consistent with that of sodium phosphates and FePO₄, respectively [51]. It further reveals that P atoms are incorporated in hematite in P-Fe₂O₃-Joule photoanode whereas they mainly exist as phosphates species in the surface of P-Fe₂O₃-Muffle photoanode.

Fourier-transform infrared (FTIR) spectroscopy has also been performed to further explore the components of as-fabricated hematite photoanodes. As shown in Fig. S4, an FTIR peak centered at 1127 cm⁻¹ corresponding to the P-O bond is observed in the P-Fe₂O₃-Muffle photoanode, which can be attributed to the formation of surface phosphates groups [52]. For the P-Fe₂O₃-Joule photoanode, an FTIR peak at 1370 cm⁻¹ originating from the stretching vibration of -COOH group is found, further confirming the deposition of oxidized carbon overlayer [53,54]. Overall, XPS, XAS, and FTIR results are indicative of the existence of an oxidized carbon overlayer with sp² carbon structure in the P-Fe₂O₃-Joule photoanode. Meanwhile, owing to the confinement of oxidized carbon overlayer, sufficient P atoms are incorporated in the hematite lattice to realize P-doping. By comparison, due to the lack of confinement and protection in the synthesis, P atoms in the P-Fe₂O₃-Muffle photoanode mainly exist as phosphates groups on the surface of hematite.

To investigate the oxidized carbon overlayer deposition and P-doping on the PEC performance of hematite, the photocurrent density-applied bias (*J-V*) plots of as-fabricated photoanodes were collected by performing the linear sweep voltammetry (LSV) measurements in a three-electrode cell. As shown in Fig. 4a, the pristine Fe₂O₃ photoanode exhibits a photocurrent density of 0.86 mA cm⁻² at 1.23 V vs. RHE. While for the optimal P-Fe₂O₃-Joule photoanode, an increased photocurrent density of 2.07 mA cm⁻² at 1.23 vs. RHE is observed. This photocurrent density is obviously higher than those of P-Fe₂O₃-muffle (1.22 mA cm⁻²) and Fe₂O₃-Joule (1.42 mA cm⁻², Fig. S5) photoanodes at the same applied bias. To further improve the PEC performance of P-Fe₂O₃-Joule photoanode, a FeNiOOH cocatalyst was loaded through a

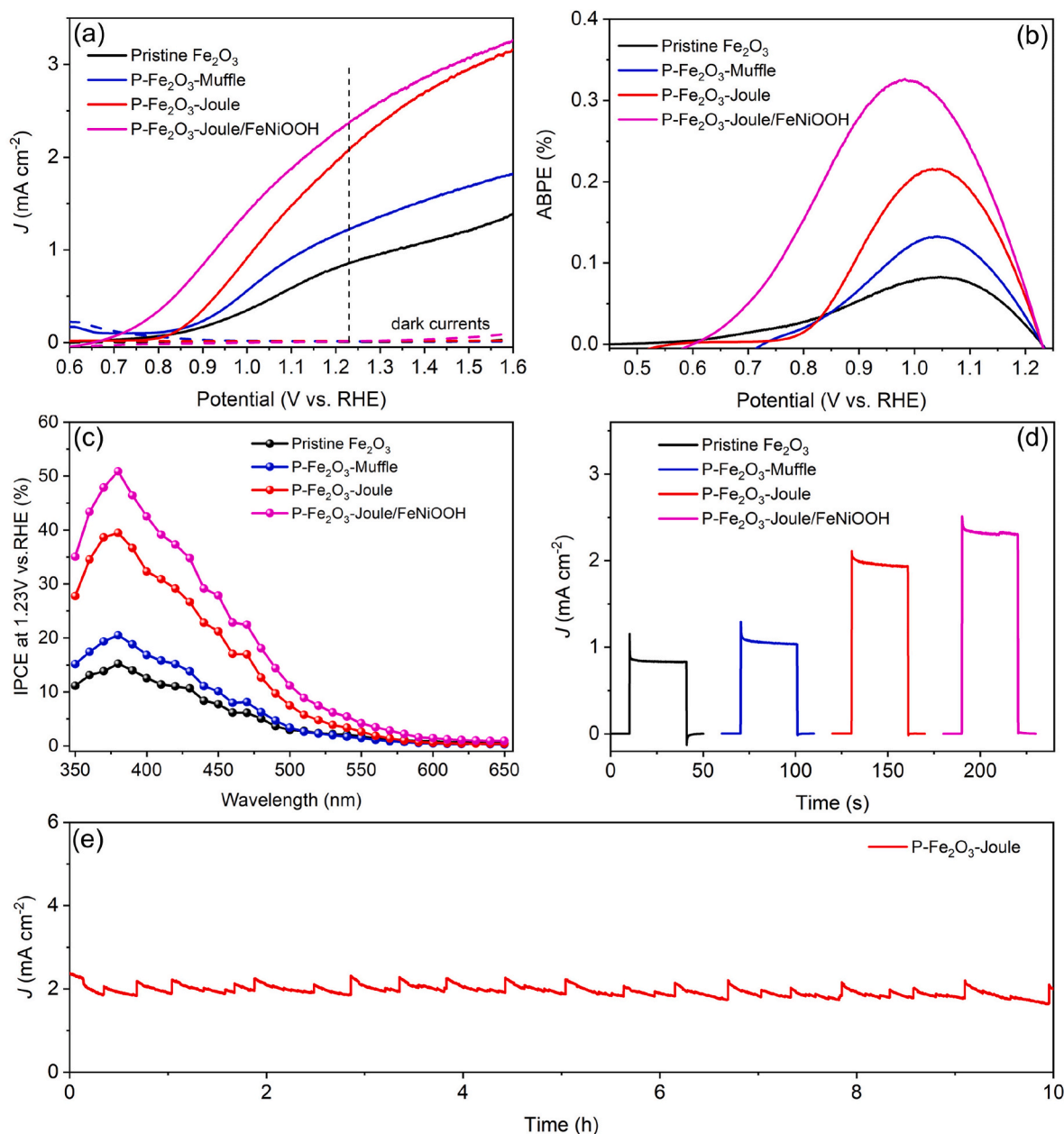


Fig. 4. (a) J - V plots, (b) ABPE, (c) IPCE, and (d) transient photocurrent curves collected at 1.23 V vs. RHE for different photoanodes, (e) PEC stability tests of P- Fe_2O_3 -Joule photoanode measured at 1.23 V vs. RHE. (A colour version of this figure can be viewed online.)

facile electrodeposition process [26]. As demonstrated in Fig. 4a, the P- Fe_2O_3 -Joule/FeNiOOH photoanode yields a further increased photocurrent density of 2.37 mA cm^{-2} at 1.23 V vs. RHE and which can be comparable with those of P-doping or carbon-coating hematite photoanodes in recent reports (Table S1).

Applied bias photon-to-current efficiency (ABPE) measurements have also been carried out to evaluate the PEC performance of as-fabricated photoanodes. As shown in Fig. 4b, the P- Fe_2O_3 -Joule photoanode exhibits a maximum ABPE of 0.21% at 1.04 V vs. RHE, which is about 1.6 and 2.6 times larger than that of pristine Fe_2O_3 (0.08% at 1.04 V vs. RHE) and P- Fe_2O_3 -Muffle (0.13% at 1.04 V vs. RHE) photoanodes, respectively. Further, the performance enhancement has been evident from the incident photon-to-current efficiency (IPCE) measured at 1.23 V vs. RHE. As observed from Fig. 4c, a higher IPCE value than those of the pristine Fe_2O_3 and P- Fe_2O_3 -Muffle samples is achieved for the P- Fe_2O_3 -Joule photoanode. Fig. 4d demonstrates the transient photocurrent curves measured at 1.23 V vs. RHE, in which the P- Fe_2O_3 -Joule

photoanode achieves the increased initial and steady-state photocurrents, agreeing well with the results of LSV measurements. Further, based on the transient photocurrent curves, the surface charge transfer efficiency for each photoanode was estimated by calculating the ratio of I_s/I_i , where I_i is defined as the transient current density just as the light is switched on and I_s refers to the steady current density just before the illumination is turned off [55,56]. After the calculation, the values of I_s/I_i of the pristine Fe_2O_3 , P- Fe_2O_3 -Muffle, P- Fe_2O_3 -Joule, and P- Fe_2O_3 -Joule/FeNiOOH photoanodes were determined to be 72%, 80%, 91%, and 92%, respectively. It is clear that the pristine Fe_2O_3 sample exhibits the lowest charge transfer efficiency and which could be attributed to the severe charge recombination in the electrode/electrolyte interface [57]. In contrast, owing to the deposition of carbon overlayer with high conductivity and abundant oxygen-functionalized carbon groups, the surface charge transfer in P- Fe_2O_3 -Joule photoanode is expedited more efficiently and consequently gains a higher I_s/I_i value than those of the pristine Fe_2O_3 and

P-Fe₂O₃-Muffle films. In addition, the P-Fe₂O₃-Joule/FeNiOOH photoanode shows a nearly same value of I_c/I_i as that of P-Fe₂O₃-Joule film and which might be ascribed to the weak effect of FeNiOOH cocatalyst on boosting the kinetics of the charge transfer process [55,58]. Fig. 4e depicts the $i-t$ curve of P-Fe₂O₃-Joule photoanode tested at 1.23 V vs. RHE under long-term light illumination. It shows that there is no obvious decay in the photocurrent density during the 10 h' illumination, suggesting its remarkable PEC stability. Fig. S6 shows the chromatogram of gas production of P-Fe₂O₃-Joule photoanode after the irradiation for 2 h at 1.23 V vs. RHE, where no CO composition from the possible carbon gasification is detected and it rules out the possibility of the increased photocurrent of the P-Fe₂O₃-Joule photoanode from the oxidation of surface carbon layer [22].

To achieve the maximum photocurrent density, the experimental conditions for the fabrication of P-Fe₂O₃-Joule photoanodes including the concentration of NaH₂PO₂ solution as well as the output electric current and the cycles of high-temperature-shock treatment have been optimized. As shown in Fig. S7, the $J-V$ curves clearly indicate that the optimal experimental conditions are 1.6 mg mL⁻¹ for NaH₂PO₂ solution, 65 A for output current, and 10 cycles for treatment times. Also, the $J-V$ plots have illustrated that a larger concentration of NaH₂PO₂ solution, higher output current, and more cycles could result in decreased photocurrent densities, which might be attributed to the damage of hematite nanostructure due to the strong etching of more P-species [59], and the increased resistivity of FTO substrate due to the higher temperature provided by larger output electrical current [60]. Overall, the PEC measurements unveil that the high-temperature-shock treatment based on the flash Joule heating technique is a feasible and effective route for improving the performance of hematite photoanode.

It is well known that the PEC performance of hematite is mainly determined by its light absorption capacity, charge separation efficiency, and charge injection efficiency for surface reaction [61]. Therefore, to understand the underlying causes of performance enhancement of P-Fe₂O₃-Joule photoanode, the light absorption abilities of as-fabricated hematite photoanodes were first investigated by conducting UV-vis spectra measurements. As shown in Fig. S8, relative to the pristine Fe₂O₃ sample, the P-Fe₂O₃-Muffle photoanode exhibits an expand light absorption range and which could be attributed to the significantly altered surface chemistry of hematite due to the presence of surface phosphates groups [62]. In contrast, on account of P-incorporation and thin characteristic of carbon overlayer, there are no obvious alters in the main absorption edges of the pristine Fe₂O₃ and P-Fe₂O₃-Joule films, ruling out the possibility of light harvesting improvement in enhancing the photoactivity of P-Fe₂O₃-Joule photoanode.

On the other hand, it is well known that alien atoms incorporation is very beneficial for facilitating the charge transport in the bulk of hematite by improving the carrier density [10–12]. Therefore, to investigate the effect of flash Joule heating in the bulk charge dynamic of hematite, the carrier densities of as-fabricated photoanodes were calculated by measuring Mott-Schottky ($M - S$) plots under dark conditions. As shown in Fig. S9, the positive slopes of $M - S$ plots indicate that the pristine Fe₂O₃, Fe₂O₃-Joule, P-Fe₂O₃-Muffle, and P-Fe₂O₃-Joule photoanodes exhibit n-type semiconducting behavior. Moreover, through the calculation (the method has been described in Supporting Information), the carrier densities of the pristine Fe₂O₃, Fe₂O₃-Joule, P-Fe₂O₃-Muffle, and P-Fe₂O₃-Joule photoanodes are determined to be $2.98 \times 10^{19} \text{ cm}^{-3}$, $2.74 \times 10^{19} \text{ cm}^{-3}$, $3.18 \times 10^{19} \text{ cm}^{-3}$, and $1.40 \times 10^{20} \text{ cm}^{-3}$, respectively. A one-order-of-magnitude increase in the carrier density further confirms the P-doping for the P-Fe₂O₃-Joule photoanode but the existence of surface phosphates groups for the P-Fe₂O₃-Muffle sample. Further, the flat band potential of the pristine Fe₂O₃ and P-Fe₂O₃-Joule photoanodes was estimated based on the $M - S$ plots. As shown in Fig. S9, the values of the flat band potential for pristine Fe₂O₃ and P-Fe₂O₃-Joule photoanodes were determined to be 0.65 and 0.69 V vs. RHE, respectively. This slight

change rules out the passivation effect of carbon overlayer in suppressing surface charge recombination [63,64].

Previous studies have demonstrated that the oxygen-functionalized carbon groups (e.g., C–O–C, C=O/COOH, and C–OH) could effectively improve the electrode hydrophilicity of carbon material [33,65], i.e., the surface charge transfer of P-Fe₂O₃-Joule photoanode can probably be boosted via depositing an oxidized carbon overlayer. Therefore, to verify this, the wettability of pristine Fe₂O₃ and P-Fe₂O₃-Joule photoanodes was first investigated by measuring the contact angle of water droplets on both films. As shown in Fig. S10, the pristine Fe₂O₃ film exhibits a contact angle of $\sim 104^\circ$, however, after the deposition of oxidized carbon overlayer, the P-Fe₂O₃-Joule photoanode shows hydrophilic surface properties with a smaller contact angle of $\sim 77^\circ$, coinciding with the expectation. Given the improved hydrophilicity and the high conductivity of carbon overlayer, the surface charge behaviors of P-Fe₂O₃-Joule photoanode could be thusly enhanced. The charge injection efficiencies (η_{inj}) of as-fabricated photoanodes were thusly evaluated by measuring the $J-V$ scans in 1 M NaOH electrolyte with and without 0.5 M H₂O₂ hole scavenger (Fig. S11). As shown in Fig. 5a, the calculation results demonstrate that P-Fe₂O₃-Joule photoanode achieves an increased η_{inj} of 79% at 1.23 V vs. RHE, relative to 57% of pristine Fe₂O₃ and 73% of P-Fe₂O₃-Muffle photoanodes. This enhancement implies that a larger proportion of photoexcited holes in the P-Fe₂O₃-Joule photoanode could be injected from the electrode into the electrolyte [66]. And it could be assigned to the deposition of carbon overlayer, its superior conductivity and abundant oxygen-functionalized carbon groups for a better electrolyte affinity greatly facilitate the interfacial charge transfer. Fig. 5b shows the η_{sep} plots of pristine Fe₂O₃, P-Fe₂O₃-Muffle, and P-Fe₂O₃-Joule photoanodes, which are calculated based on the $J-V$ scans with and without H₂O₂ scavenger (Fig. S11) as well as the integrated current densities (Fig. S12). It is clear that since P atoms mostly exist as surface phosphates groups and have no significant effects on the bulk properties of hematite, there is no obvious improvement in the charge separation efficiencies of pristine Fe₂O₃ and P-Fe₂O₃-Muffle photoanodes. On the contrary, on account of the remarkably increased carrier density from P-incorporation, the P-Fe₂O₃-Joule photoanode achieves a higher value of η_{sep} of 31% at 1.23 V vs. RHE than 19% of the pristine Fe₂O₃ sample.

To gain more insights into the working mechanism of the P-Fe₂O₃-Joule photoanode, intensity modulated photocurrent spectroscopy (IMPS) and electrochemical impedance spectroscopy (EIS) were conducted to probe charge separation and transfer kinetics of as-obtained photoanodes. Fig. S13 shows the IMPS results of pristine Fe₂O₃, P-Fe₂O₃-Muffle, and P-Fe₂O₃-Joule photoanodes that were measured at different biases. According to these spectra, the rate constants for charge transfer (k_{tr}) and recombination (k_{rec}) for these three samples were calculated. As shown in Fig. 5c and d, there are small differences in the values of k_{rec} , while the difference in k_{tr} is significant and the P-Fe₂O₃-Joule photoanode has the largest k_{tr} values. This finding strongly suggests that the improved surface charge-transfer efficiency rather than the suppressed surface carrier recombination in the presence of carbon overlayer is primarily responsible for the improved PEC performance of P-Fe₂O₃-Joule photoanode [67,68]. Fig. 5d displays the EIS spectra at 1.23 V vs. RHE under AM 1.5G illumination for pristine Fe₂O₃, P-Fe₂O₃-Muffle, and P-Fe₂O₃-Joule photoanodes, where the P-Fe₂O₃-Joule photoanode shows the smallest radius of Nyquist plot than those of pristine Fe₂O₃ and P-Fe₂O₃-Muffle films, indicating the fastest charge transfer. To probe the charge dynamics in more detail, Nyquist plots are fitted using the equivalent circuit (EC) in Fig. S14. In the EC model of pristine Fe₂O₃ and P-Fe₂O₃-Muffle photoanodes (Fig. S14a), R_s represents the series resistance; R_{trap} and C_{bulk} stand for the charge transport resistance from the bulk electrode to surface states and the capacitance of the bulk electrode, respectively; while R_{ct} and C_{trap} correspond to the charge transfer resistance across electrode/electrolyte interface and the trap capacitance of the surface states, respectively [9,13,69]. For the P-Fe₂O₃-Joule photoanode, since the

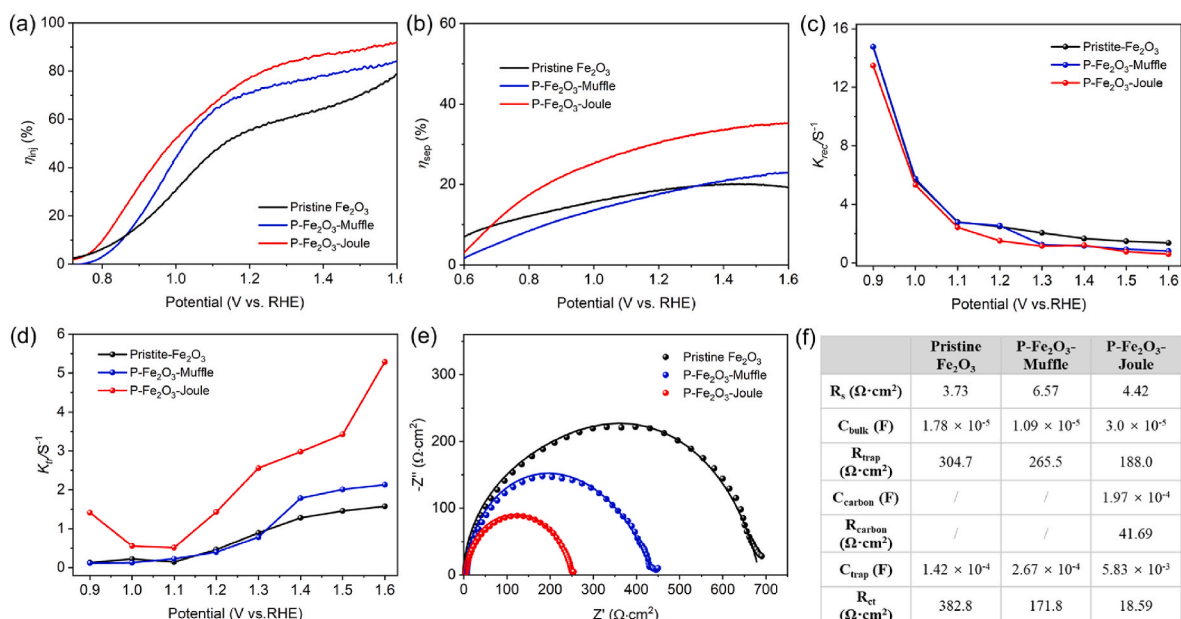


Fig. 5. (a) Charge injection efficiencies (η_{inj}), (b) charge separation efficiencies (η_{sep}), (c) surface charge recombination rate constants (k_{rec}), (d) surface charge transfer rate constants (k_{tr}), (e) Nyquist plots, and (f) fitting results for pristine Fe₂O₃, P-Fe₂O₃-Muffle, and P-Fe₂O₃-Joule photoanodes. (A colour version of this figure can be viewed online.)

charge transfer takes place mainly through the carbon coating layer, an EC model containing another RC unit that corresponds to the charge dynamics in the carbon coating layer was adopted (Fig. S14b) [70]. Fig. 5d illustrates the fitting results of as-fabricated hematite photoanodes. It is clear that compared with the pristine Fe₂O₃ film, the P-Fe₂O₃-Joule photoanode exhibits an increased C_{bulk} and a dramatically reduced R_{trap}, indicating a facilitated charge transport in the bulk electrode. Given the P-doping confined by carbon overlayer, the improved bulk charge dynamic of the P-Fe₂O₃-Joule photoanode can be attributed to the enhanced bulk charge transport and separation owing to the greatly increased carrier density [13,69]. By contrast, since the P atoms mainly exist as the phosphate groups on the hematite surface, the bulk charge behaviors of the P-Fe₂O₃-Muffle photoanode don't alter essentially. Also, the P-Fe₂O₃-Joule photoanode exhibits a much lower R_{ct} value of 18.59 Ω than 382.8 Ω of pristine Fe₂O₃ and 171.8 Ω of P-Fe₂O₃-Muffle samples, manifesting the significantly reduced charge transfer resistance at electrode/electrolyte interface [9,13,69]. Meanwhile, the largest C_{trap} than those of pristine Fe₂O₃ and P-Fe₂O₃-Joule samples is also achieved for the P-Fe₂O₃-Joule photoanode, indicating more surface states for the accelerated PEC water oxidation process [9,13,69]. In short, IMPS and EIS measurements reveal that for the P-Fe₂O₃-Joule photoanode, P-incorporation and carbon overlayer deposition can not only facilitate surface/bulk charge dynamics but also speed up surface water oxidation.

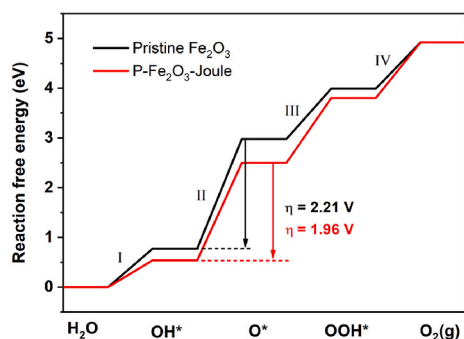
To rationalize the role of oxidized carbon overlayer in accelerating surface water oxidation of hematite, the Tafel slopes of pristine Fe₂O₃ and P-Fe₂O₃-Joule photoanodes were measured in the dark. For (photo) electrocatalysts, Tafel plots are generally utilized to determine the surface reaction kinetics of electrodes. As shown in Fig. S15, the pristine Fe₂O₃ and P-Fe₂O₃-Joule photoanode exhibit identical Tafel slopes, indicating that the oxidized carbon overlayer does not act as a cocatalyst to alter the OER kinetics of hematite [71,72]. On the other hand, recent studies have shown that the carbon coating layer could mediate the adsorption energies of water oxidation intermediates on inner metal-based electrocatalysts to boost the OER activity [73,74]. Therefore, to deeply understand how the oxidized carbon overlayer enhances the OER activity of P-Fe₂O₃-Joule photoanode, the adsorption behaviors of key intermediates (*O, *OH, and *OOH) of water oxidation on pristine Fe₂O₃ and P-Fe₂O₃-Joule photoanodes were investigated by

performing density functional theory (DFT) calculations (the method is reported in Supporting Information). As shown in Fig. 6, on the (110) surface of pristine Fe₂O₃, the adsorption free energies of *O, *OH, and *OOH are 2.98 eV, 0.77 eV, and 3.99 eV, respectively. While on the (110) surface of P-Fe₂O₃-Joule photoanode, the adsorption free energies of *O, *OH, and *OOH turn into 2.5 eV, 0.54 eV, and 3.8 eV, respectively. It is clear that adsorption free energies of *O, *OH, and *OOH intermediates are lower on the P-Fe₂O₃-Joule (110) surface than on the pristine Fe₂O₃ (110) surface, indicating that these intermediates are much more strongly adsorbed on P-Fe₂O₃-Joule (110) surface [75]. It also means that the oxidized carbon overlayer could enhance the adsorption strength of water oxidation intermediates on the Fe sites. The free energies of OER reaction steps of pristine Fe₂O₃ and P-Fe₂O₃-Joule photoanodes have also been calculated. As shown in Fig. 6, the reaction from *OH to *O is the rate-determining step in the pristine Fe₂O₃ and P-Fe₂O₃-Joule photoanodes and the corresponding theoretical overpotential are 2.21 V and 1.96 V, respectively. This lower overpotential of P-Fe₂O₃-Joule photoanode manifests the accelerated OER kinetics and which mainly results from the enhanced adsorption of water oxidation intermediates on the surface.

Based on the above analyses, the performance enhancement of P-Fe₂O₃-Joule photoanode can be assigned to the following distinct benefits (Fig. 7): (i) on account of the high conductivity and abundant oxygen-functionalized carbon groups, the oxidized carbon overlayer enables a better electrolyte affinity with facilitated interfacial charge transfer; (ii) the oxygen-functionalized carbon groups are favorable for promoting the surface water oxidation activity by mediating the adsorption strength of water oxidation intermediates; (iii) owing to the confinement of carbon overlayer, sufficient P atoms are incorporated in the hematite to significantly improve the bulk charge transport and separation via increasing the carrier density.

4. Conclusions

In summary, an oxidized carbon overlayer confined P-doping hematite photoanode is successfully synthesized through a facile high-temperature-shock treatment based on a flash Joule heating technique. On account of the high conductivity and abundant oxygen-functionalized carbon groups of carbon overlayer, surface charge



Reaction equations for each step:

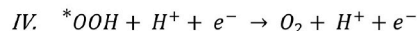
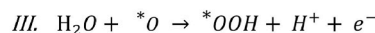
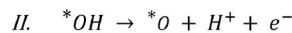


Fig. 6. Reaction free-energy diagram of the water oxidation intermediates on pristine Fe_2O_3 and P- Fe_2O_3 -Joule photoanodes. (A colour version of this figure can be viewed online.)

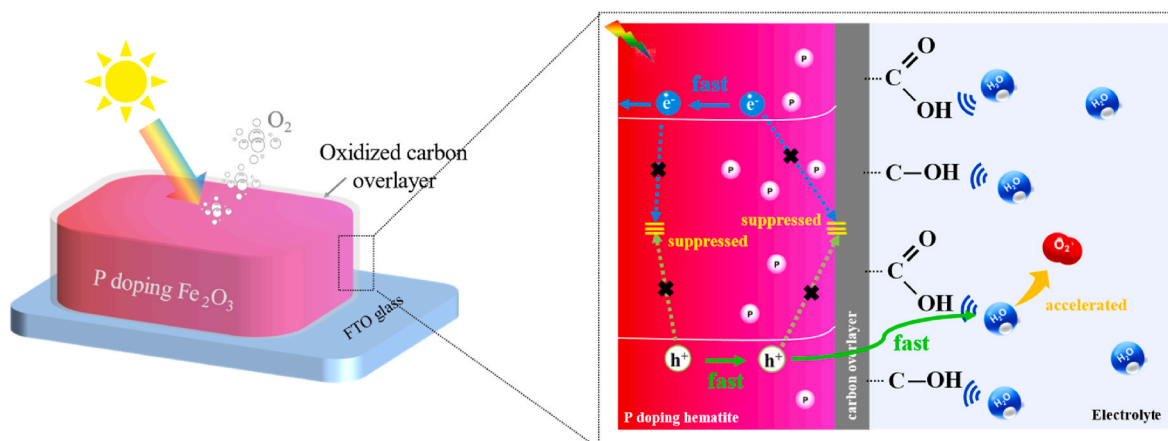


Fig. 7. Illustration of the working mechanism of P- Fe_2O_3 -Joule photoanode. (A colour version of this figure can be viewed online.)

transfer and the water oxidation activity of P- Fe_2O_3 -Joule photoanode are greatly facilitated. Moreover, owing to the confinement of carbon overlayer, sufficient P atoms are incorporated in the hematite that greatly promotes the bulk charge transport/separation via increasing the carrier density. Consequently, owing to the multiple effects, an enhanced photocurrent density of 2.07 mA cm^{-2} at 1.23 V vs. RHE is obtained for the P- Fe_2O_3 -Joule photoanode. This work offers a novel, effective and facile strategy for the fabrication of efficient hematite photoanodes.

CRedit authorship contribution statement

Guoqing Li: Resources, Writing – review & editing. **Wei Zhang:** DFT calculation. **Kaiqi Nie:** Acquisition & analysis of XAS data. **Xiaoxin Lv:** Resources, Writing – review & editing, Supervision. **Jiujun Deng:** Resources, Writing – review & editing, Supervision, Funding acquisition. **Hongbing Ji:** Writing – review & editing, Supervision.

Declaration of competing interest

The authors declare that they have no known competing financial interests or personal relationships that could have appeared to influence the work reported in this paper.

Acknowledgments

We acknowledge the financial support from Jiangsu Key Laboratory for Carbon-Based Functional Materials & Devices, Soochow University (KJS2206), the China Postdoctoral Science Foundation (2020T130754), and the Scientific Research Startup Foundation of Jiangsu University

(2021JDG025, 18JDG019). We acknowledge the support from Beijing Synchrotron Radiation Facility (BSRF) and National Synchrotron Radiation Laboratory (NSRL, Beamlines MCD-A and MCD-B (Soochow Beamline for Energy Materials)) for the XAS experiments.

Appendix A. Supplementary data

Supplementary data to this article can be found online at <https://doi.org/10.1016/j.carbon.2023.118444>.

References

- [1] K. Sivula, K.R. Vande, Semiconducting materials for photoelectrochemical energy conversion, *Nat. Rev. Mater.* 1 (2016), 15010.
- [2] R. Passalacqua, S. Perathoner, G. Centi, Semiconductor, molecular and hybrid systems for photoelectrochemical solar fuel production, *J. Energy Chem.* 26 (2017) 219–240.
- [3] K. Sivula, F.F. Le, M. Grätzel, Solar water splitting: progress using hematite ($\alpha\text{-Fe}_2\text{O}_3$) photoelectrodes, *ChemSusChem* 4 (2011) 432–449.
- [4] C. Li, Z. Luo, T. Wang, J. Gong, Surface, bulk, and interface: rational design of hematite architecture toward efficient photo-electrochemical water splitting, *Adv. Mater.* 30 (2018), 1707502, 25.
- [5] J. Deng, Q. Zhang, X. Lv, D. Zhang, H. Xu, D. Ma, et al., Understanding photoelectrochemical water oxidation with X-ray absorption spectroscopy, *ACS Energy Lett.* 53 (2020) 975–993.
- [6] J. Li, H. Chen, C.A. Triana, G.R. Patzke, Hematite photoanodes for water oxidation: electronic transitions, carrier dynamics, and surface energetics, *Angew. Chem., Int. Ed.* 60 (2021), 18380.
- [7] P. Peerakiatkhajohn, J.-H. Yun, H. Chen, M. Lyu, T. Butburee, L. Wang, Stable hematite nanosheet photoanodes for enhanced photoelectrochemical water splitting, *Adv. Mater.* 28 (2016) 6405–6410.
- [8] Y. Choi, D. Jeon, Y. Choi, D. Kim, N. Kim, M. Gu, et al., Interface engineering of hematite with nacre-like catalytic multilayers for solar water oxidation, *ACS Nano* 13 (2019) 467–475.

- [9] J. Deng, Y. Li, Y. Xiao, K. Feng, C. Lu, K. Nie, et al., Improved water oxidation of $\text{Fe}_2\text{O}_3/\text{Fe}_2\text{TiO}_5$ photoanode by functionalizing with a hydrophilic organic hole storage overlayer, *ACS Catal.* 12 (2022) 7833–7842.
- [10] T.S. Koh, P. Anushkaran, W.-S. Chae, H.H. Lee, S.H. Choi, J.S. Jang, Gradient Si- and Ti-doped Fe_2O_3 hierarchical homojunction photoanode for efficient solar water splitting: effect of facile microwave-assisted growth of Si-FeOOH on Ti-FeOOH nanocorals, *J. Energy Chem.* 77 (2023) 27–37.
- [11] M. Li, Y. Yang, Y. Ling, W. Qiu, F. Wang, T. Liu, et al., Morphology and doping engineering of Sn-doped hematite nanowire photoanodes, *Nano Lett.* 17 (2017) 2490–2495.
- [12] S. Shen, P. Guo, D.A. Wheeler, J. Jiang, S.A. Lindley, C.X. Kronawitter, et al., Physical and photoelectrochemical properties of Zr-doped hematite nanorod arrays, *Nanoscale* 5 (2013) 9867–9874.
- [13] H.-J. Ahn, K.-Y. Yoon, M.-J. Kwak, J. Park, J.-H. Jang, Boron doping of metal-doped hematite for reduced surface recombination in water splitting, *ACS Catal.* 8 (2018) 11932–11939.
- [14] Z. Luo, C. Li, S. Liu, T. Wang, J. Gong, Gradient doping of phosphorus in Fe_2O_3 nanoarray photoanodes for enhanced charge separation, *Chem. Sci.* 8 (2017) 91–100.
- [15] Q. Rui, L. Wang, Y. Zhang, C. Feng, B. Zhang, S. Fu, et al., Synergistic effects of P-doping and a MnO_2 cocatalyst on Fe_2O_3 nanorod photoanodes for efficient solar water splitting, *J. Mater. Chem. A* 6 (2018) 7021–7026.
- [16] P.C. Melissa, M. Li, W. Li, M.C. Jeremie, D. Wang, Y. Li, et al., The role of graphene as an overlayer on nanostructured hematite photoanodes for improved solar water oxidation, *Mater. Today Energy* 8 (2018) 8–14.
- [17] P. Zhang, T. Wang, X. Chang, L. Zhang, J. Gong, Synergistic cocatalytic effect of carbon nanodots and Co_3O_4 nanoclusters for the photoelectrochemical water oxidation on hematite, *Angew. Chem., Int. Ed.* 55 (2016) 5851–5855.
- [18] J. Deng, X. Lv, J. Gao, A. Pu, M. Li, X. Sun, et al., Facile synthesis of carbon-coated hematite nanostructures for solar water splitting, *Energy Environ. Sci.* 6 (2013) 1965–1970.
- [19] S.A. Carminati, A. do Nascimento Barbosa, A.L.M. de Freitas, F.L. Freire Jr., F. L. Souza, A.F. Nogueira, Unraveling the role of single layer graphene as overlayer on hematite photoanodes, *J. Catal.* 372 (2019) 109–118.
- [20] P. Wu, H. Wang, Y. Li, S. Xue, Q. Wu, Understanding the role of uniformly coated carbon overlayers in hematite nanorod photoanodes, *Sol. Energy* 208 (2020) 728–737.
- [21] T.-T. Kong, J. Huang, X.-J. Jia, W.-Z. Wang, Y. Zhou, Z.-G. Zou, Nitrogen-doped carbon nanolayer coated hematite nanorods for efficient photoelectrocatalytic water oxidation, *Appl. Catal., B* 275 (2020), 119113.
- [22] H. Lan, Y. Xia, K. Feng, A. Wei, Z. Kang, J. Zhong, Co-doped carbon layer to lower the onset potential of hematite for solar water oxidation, *Appl. Catal., B* 258 (2019), 117962.
- [23] N. Cheng, Q. Liu, J. Tian, Y. Xue, M.A. Abdullah, H. Jiang, et al., Acidically oxidized carbon cloth: a novel metal-free oxygen evolution electrode with high catalytic activity, *Chem. Commun.* 51 (2015) 1616–1619.
- [24] X. Lu, W.-L. Yim, H.R.S. Bryan, C. Zhao, Electrocatalytic oxygen evolution at surface-oxidized multiwall carbon nanotubes, *J. Am. Chem. Soc.* 137 (2015) 2901–2907.
- [25] S.T. Aziz, B. Malik, H.K. Sadhanala, A. Gedanken, M. Noked, G.D. Nessim, Nickel-rich phosphide (Ni_2P) nanosheets coupled with oxidized multiwalled carbon nanotubes for oxygen evolution, *ACS Appl. Nano Mater.* 3 (2020) 10914–10921.
- [26] Z. Liu, Z. Zhao, Y. Wang, S. Dou, D. Yan, D. Liu, et al., In situ exfoliated, edge-rich, oxygen-functionalized graphene from carbon fibers for oxygen electrocatalysis, *Adv. Mater.* 29 (2017), 1606207.
- [27] S. Dou, J. Xu, X. Cui, W. Liu, Z. Zhang, Y. Deng, et al., High-temperature shock enabled nanomanufacturing for energy-related applications, *Adv. Energy Mater.* 10 (2020), 2001331.
- [28] W. Chen, C. Ge, J.T. Li, J.L. Beckham, Z. Yuan, K.M. Wyss, et al., Heteroatom-doped flash graphene, *ACS Nano* 16 (2022) 6646–6656.
- [29] S. Zhu, F. Zhang, H.-G. Lu, J. Sheng, L. Wang, S.-D. Li, et al., Flash nitrogen-doped graphene for high-rate supercapacitors, *ACS Mater. Lett.* 4 (2022) 1863–1871.
- [30] T. Jiao, C. Lu, D. Zhang, K. Feng, S. Wang, Z. Kang, et al., Bi-functional Fe_2ZrO_5 modified hematite photoanode for efficient solar water splitting, *Appl. Catal., B* 269 (2020), 118768.
- [31] J. Deng, Q. Zhang, K. Feng, H. Lan, J. Zhong, M. Chaker, et al., Efficient photoelectrochemical water oxidation on hematite with fluorine-doped FeOOH and FeNiOOH as dual cocatalysts, *ChemSusChem* 11 (2018) 3783–3789.
- [32] Z. Panagiota, S. Konstantinos, M. Efstathia, B. Maria, M. Roberto, P. Michaela, et al., A facile approach to hydrophilic oxidized fullerenes and their derivatives as cytotoxic agents and supports for nanobiocatalytic systems, *Sci. Rep.* 10 (2020) 8244.
- [33] Z. Liu, Z. Zhao, Y. Wang, S. Dou, D. Yan, D. Liu, et al., In situ exfoliated, edge-rich, oxygen-functionalized graphene from carbon fibers for oxygen electrocatalysis, *Adv. Mater.* 29 (2017), 1606207.
- [34] Y. Zhang, S. Jiang, W. Song, P. Zhou, H. Ji, W. Ma, et al., Nonmetal P-doped hematite photoanode with enhanced electron mobility and high water oxidation activity, *Energy Environ. Sci.* 8 (2015) 1231–1236.
- [35] C. Liu, Y. Xu, H. Luo, W. Wang, Q. Liang, Z. Chen, Synthesis and photoelectrochemical properties of $\text{CoOOH}/\text{phosphorus-doped hematite}$ photoanodes for solar water oxidation, *Chem. Eng. J.* 363 (2019) 23–32.
- [36] Z. Wang, L. Li, M. Liu, T. Miao, X. Ye, S. Meng, et al., A new phosphidation route for the synthesis of NiP_x and their cocatalytic performances for photocatalytic hydrogen evolution over $\text{g-C}_3\text{N}_4$, *J. Energy Chem.* 48 (2020) 241–249.
- [37] C. Xia, Y. Li, H. Kim, K. Kim, W.-S. Choe, J.-K. Kim, et al., A highly activated iron phosphate over-layer for enhancing photoelectrochemical ammonia decomposition, *J. Hazard Mater.* 408 (2021), 124900.
- [38] X. Bu, Y. Gao, S. Zhang, Y. Tian, Amorphous cerium phosphate on P-doped Fe_2O_3 nanosheets for efficient photoelectrochemical water oxidation, *Chem. Eng. J.* 355 (2019) 910–919.
- [39] D. Wu, Z. Zhang, Simultaneous non-metal doping and cocatalyst decoration for efficient photoelectrochemical water splitting on hematite photoanodes, *Electrochim. Acta* 282 (2018) 48–55.
- [40] Y. Kang, K.-Y. Yoon, J.-E. Lee, J. Park, S. Chauhe, J.-H. Jang, Meso-pore generating P doping for efficient photoelectrochemical water splitting, *Nano Energy* 107 (2023), 108090.
- [41] Y. Nie, Y. Bai, J. Gao, J. Liu, G. Zhao, T. Xie, et al., Imaging the electronic structure of carbon nanotubes decorated with Fe_2O_3 nanoparticles, *Appl. Surf. Sci.* 273 (2013) 386–390.
- [42] G.L. Kenneth, I.S. Michela, M.D. Wesley, A.A. Jessica, W.D. Scott, Synchrotron based NEXAFS study on nitrogen doped hydrothermal carbon: insights into surface functionalities and formation mechanisms, *Carbon* 114 (2017) 566–578.
- [43] Y. Ye, E.T. James, C.H. Wu, Y.-S. Liu, C. Du, J.-W. Jang, et al., Strong O 2p-Fe 3d hybridization observed in solution-grown hematite films by soft X-ray spectroscopies, *J. Phys. Chem. Lett.* 13 (2022) 4207–4214.
- [44] S. Yang, D. Wang, G. Liang, Y.M. Yiu, J. Wang, L. Liu, et al., Soft X-ray XANES studies of various phases related to LiFePO_4 based cathode materials, *Energy Environ. Sci.* 5 (2012) 7007–7016.
- [45] H.-W. Chang, Y. Fu, W.-Y. Lee, Y.-R. Lu, Y.-C. Huang, J.-L. Chen, et al., Visible light-induced electronic structure modulation of Nb- and Ta-doped $\alpha\text{-Fe}_2\text{O}_3$ nanorods for effective photoelectrochemical water splitting, *Nanotechnology* 29 (2018), 064002.
- [46] Y. Fu, C.-L. Dong, W.-Y. Lee, J. Chen, P. Guo, L. Zhao, et al., Nb-doped hematite nanorods for efficient solar water splitting: electronic structure evolution versus morphology alteration, *Chem. Nano Mater.* 2 (2016) 704–711.
- [47] Z. Liu, J. Liang, Q. Song, Y. Li, Z. Zhang, M. Zhou, et al., Construction atomic-level N-P charge transfer channel for boosted CO_2 photoreduction, *Appl. Catal., B* 328 (2023), 122472.
- [48] W. Xiong, J. Peng, Y. Hu, Use of X-ray absorption near edge structure (XANES) to identify physiosorption and chemisorption of phosphate onto ferrihydrite-modified diatomite, *J. Colloid Interface Sci.* 368 (2012) 528–532.
- [49] G. Pereira, A. Lachenwitzer, D. Munoz-Paniagua, M. Kasrai, P.R. Norton, M. Abrecht, et al., The role of the cation in antiwear films formed from ZDDP on 52100 steel, *Tribol. Lett.* 23 (2006) 109–119.
- [50] M.A. Nicholls, P.R. Norton, G.M. Bancroft, M. Kasrai, T. Do, B.H. Frazer, et al., Nanometer scale chemomechanical characterization of antiwear films, *Tribol. Lett.* 17 (2004) 205–216.
- [51] J. Kruse, P. Leinweber, K.-U. Eckhardt, F. Godlinski, Y. Hu, L. Zuin, Phosphorus $L_{2,3}$ -edge XANES: overview of reference compounds, *J. Synchrotron Radiat.* 16 (2009) 247–259.
- [52] J.Y. Kim, J.-W. Jang, D.H. Youn, G. Magesh, J.S. Lee, A stable and efficient hematite photoanode in a neutral electrolyte for solar water splitting: towards stability engineering, *Adv. Energy Mater.* 4 (2014), 1400476.
- [53] S. Han, Y. Dina, F. Teng, A. Yao, Q. Leng, Determination of chloropropanol with an imprinted electrochemical sensor based on multi-walled carbon nanotubes/metal-organic framework composites, *RSC Adv.* 11 (2021) 18468–18475.
- [54] F. Ornella, S.-C. Santiago, B. Sergio, L.R. Maria, C. Giacomo, Structural characterization of charcoal size-fractions from a burnt Pinus pinea forest by FT-IR, Raman and surface-enhanced Raman spectroscopies, *J. Mol. Struct.* 994 (2011) 155–162.
- [55] T. Wang, L. Gao, P. Wang, X. Long, H. Chai, F. Li, et al., Dual-doping in the bulk and the surface to ameliorate the hematite anode for photoelectrochemical water oxidation, *J. Colloid Interface Sci.* 624 (2022) 60–69.
- [56] Z. Zhou, S. Wu, C. Xiao, L. Li, X. Li, Underlayer engineering into the Sn-doped hematite photoanode for facilitating carrier extraction, *Phys. Chem. Chem. Phys.* 22 (2020) 7306–7313.
- [57] P. Anushkaran, L.K. Dhandole, W.-S. Chae, H.H. Lee, S.H. Choi, J. Ryu, et al., Synergistic effect of titanium oxide underlayer and interlayer on zirconium-doped zinc ferrite photoanode for photoelectrochemical water splitting, *Int. J. Hydrogen Energy* 47 (2022) 32015–32030.
- [58] J. Xiao, L. Fan, Z. Huang, J. Zhong, F. Zhao, K. Xu, et al., Functional principle of the synergistic effect of co-loaded Co-Pi and FeOOH on Fe_2O_3 photoanodes for photoelectrochemical water oxidation, *Chin. J. Catal.* 41 (2020) 1761–1771.
- [59] S. Shao, Y. Xiao, J. Yang, X. Lv, K. Feng, Y. Xia, et al., In-situ surface reconstruction in Pt and P co-treated hematite for enhanced water oxidation, *Chem. Eng. J.* 413 (2021), 127416.
- [60] Y. Ling, G. Wang, A.W. Damon, J.Z. Zhang, Y. Li, Sn-doped hematite nanostructures for photoelectrochemical water splitting, *Nano Lett.* 11 (2011) 2119–2125.
- [61] Z. Wang, L. Wang, Progress in designing effective photoelectrodes for solar water splitting, *Chin. J. Catal.* 39 (2018) 369–378.
- [62] W. Sun, Q. Meng, L. Jing, D. Liu, Y. Cao, Facile synthesis of surface-modified nanosized $\alpha\text{-Fe}_2\text{O}_3$ as efficient visible photocatalysts and mechanism insight, *J. Phys. Chem. C* 117 (2013) 1358–1365.
- [63] H. Lim, J.Y. Kim, E.J. Evans, A. Rai, J.-H. Kim, B.R. Wygant, et al., Activation of a nickel-based oxygen evolution reaction catalyst on a hematite photoanode via incorporation of cerium for photoelectrochemical water oxidation, *ACS Appl. Mater. Interfaces* 9 (2017) 30654–30661.

- [64] L. Xi, P.S. Bassi, S.Y. Chiam, W.F. Mak, P.D. Tran, J. Barber, et al., Surface treatment of hematite photoanodes with zinc acetate for water oxidation, *Nanoscale* 4 (2012) 4430–4433.
- [65] K. Kordek, L. Jiang, K. Fan, Z. Zhu, L. Xu, M. Al-Mamun, et al., Two-step activated carbon cloth with oxygen-rich functional groups as a high-performance additive-free air electrode for flexible zinc-air batteries, *Adv. Energy Mater.* 9 (2019), 1802936.
- [66] L. Xi, S.Y. Chiam, F.M. Wai, D.T. Phong, B. James, C.J.L. Say, et al., A novel strategy for surface treatment on hematite photoanode for efficient water oxidation, *Chem. Sci.* 4 (2013) 164–169.
- [67] Z. Zhou, S. Wu, L. Li, L. Li, X. Li, Regulating the silicon/hematite microwire photoanode by the conformal Al_2O_3 intermediate layer for water splitting, *ACS Appl. Mater. Interfaces* 11 (2019) 5978–5988.
- [68] Z. Wang, J. Rong, J. Lv, R. Chong, L. Zhang, L. Wang, et al., Chelation-mediated in-situ formation of ultrathin cobalt (oxy)hydroxides on hematite photoanode towards enhanced photoelectrochemical water oxidation, *J. Energy Chem.* 56 (2021) 152–161.
- [69] J. Xiao, H. Huang, Q. Huang, L. Zhao, X. Li, X. Hou, et al., Suppressing the electron-hole recombination rate in hematite photoanode with a rapid cooling treatment, *J. Catal.* 350 (2017) 48–55.
- [70] H. Zhang, D. Li, W.J. Byun, X. Wang, T.J. Shin, H.Y. Jeong, et al., Gradient tantalum-doped hematite homojunction photoanode improves both photocurrents and turn-on voltage for solar water splitting, *Nat. Commun.* 11 (2020) 4622.
- [71] X. Yang, R. Liu, C. Du, P. Dai, Z. Zheng, D. Wang, Improving hematite-based photoelectrochemical water splitting with ultrathin TiO_2 by atomic layer deposition, *ACS Appl. Mater. Interfaces* 6 (2014) 12005–12011.
- [72] M.G. Ahmed, I.E. Kretschmer, T.A. Kandel, A.Y. Ahmed, F.A. Rashwan, D. W. Bahnemann, A facile surface passivation of hematite photoanodes with TiO_2 overlayers for efficient solar water splitting, *ACS Appl. Mater. Interfaces* 7 (2015) 24053–24062.
- [73] Y. Tan, Z. Zhang, Z. Lei, L. Yu, W. Wu, Z. Wang, et al., Electronic modulation optimizes OH^* intermediate adsorption on Co- N_x -C sites via coupling CoNi alloy in hollow carbon nanopolyhedron toward efficient reversible oxygen electrocatalysis, *Appl. Catal., B* 304 (2022), 121006.
- [74] X. Cui, P. Ren, D. Deng, J. Deng, X. Bao, Single layer graphene encapsulating non-precious metals as high-performance electrocatalysts for water oxidation, *Energy Environ. Sci.* 9 (2016) 123–129.
- [75] J. Cai, X. Tang, L. Xu, H. Li, H. Zhu, X. Li, et al., Accelerated oxygen evolution kinetics on hematite by Zn^{2+} for boosting the photoelectrochemical water oxidation, *J. Alloys Compd.* 919 (2022), 165853.